plant, and we intend to test our detector for such a purpose as well.

ACKNOWLEDGMENT

The authors would like to thank the following persons for their support: Mr. Yoshihiro Nakamura of the Institute of Multidisciplinary Research for Advanced Materials (IMRAM), Tohoku University, and Mr. Hiroshi Uemura, Ms. Keiko Toguchi, Ms. Megumi Sasaki, and Ms. Yumiko Saijo of IMR.

REFERENCES

[1] S. R. Cherry, Y. Shao, R. W. Silverman, K. Meadors, S. Siegel, A. Chatziioannou, J. W. Young, W. F. Jones, J. C. Moyers, D. Newport, A. Boutefnouchet, T. H. Farquhar, M. Andreaco, M. J. Paulus, D. M. Binkley, R. Nutt, and M. E. Phelps, "MicroPET: A high resolution PET scanner for imaging small animals," *IEEE Trans. Nucl. Sci.*, vol. 44, no. 3, pp. 1161–1166, Jun. 1997.

[2] A. P. Jeavons, R. A. Chandler, and C. A. R. Dettmar, "A 3D HIDAC-PET camera with sub-millimetre resolution for imaging small animals," *IEEE Trans. Nucl. Sci.*, vol. 46, no. 3, pp. 468–473, Jun. 1999.

[3] P. Vaska, C. L. Woody, D. J. Schlyer, S. Shokouhi, S. P. Stoll, J.-F. Pratte, P. O'Connor, S. S. Junnarkar, S. Rescia, B. Yu, M. Purschke, A. Kandasamy, A. Villanueva, A. Kriplani, V. Radeka, N. Volkow, R. Lecomte, and R. Fontaine, "RatCAP: Miniaturized head-mounted PET for conscious rodent brain imaging," *IEEE Trans. Nucl. Sci.*, vol. 51, no. 5, pp. 2718–2722, Oct. 2004.

[4] K. Ziemons, E. Auffray, R. Barbier, G. Brandenburg, P. Bruyndonckx, Y. Choi, D. Christ, N. Costes, Y. Declais, O. Devroede, C. Dujardin, A. Fedorovd, U. Heinrichs, M. Korjik, M. Krieguer, C. Kuntner, G. Largeron, C. Lartizien, H. Larue, P. Lecoq, S. Leonard, J. Marteau, C. Morel, J. B. Mosset, C. Parl, C. Pedrini, A. G. Petrosyan, U. Pietrzyk, M. Rey, S. Saladino, S.-M. Sappey-Marinier, L. Simon, M. Streun, S. Tavernier, and J. M. Vieira, "The ClearPET project: development of a 2nd generation highperformance " small animal PET scanner," *Nucl. Instrum. Methods A*, vol. 537, pp. 307–311, Jan. 2005.

[5] P. Sempere Roldan, E. Chereul, O. Dietzel, L. Magnier, C. Pautrot, L. Rbah, D. Sappey-Marinier, A. Wagner, L. Zimmer, M. Janier, V. Tarazona, and G. Dietzel, "Raytest ClearPET, a new generation small animal PET scanner," *Nucl. Instrum. Methods A*, vol. 571, pp. 498–501, Feb. 2007.

[6] S. Surti, J. S. Karp, A. E. Perkins, C. A. Cardi, M. E. Daube-Witherspoon, A. Kuhn, and G. Muehllehner, "Imaging performance of a-PET: A small animal PET camera," *IEEE Trans. Med. Imag.*, vol. 24, no. 7, pp. 844–852, Jul. 2005.

[7] K. Chien-Min, X. Qingguo, D. Yun, W. Lu, and C. Chin-Tu, "A High-Sensitivity small-animal PET scanner: Development and initial performance measurements," *IEEE Trans. Nucl. Sci.*, vol. 56, no. 5, pp. 267–2688, Oct. 2009.

[8] H. Alva-Sanchez, T. Murrieta, E. Moreno-Barbosa, M. E. Brandan, C. Ruiz-Trejo, A. Martinez-Davalos, and M. Rodriguez-Villafuerte, "A Small-Animal PET system based on LYSO crystal arrays, PS-PMTs and a PCI DAQ board," *IEEE Trans. Nucl. Sci.*, vol. 57, no. 1, pp. 85–93, Feb. 2010.

[9] S. Yamamoto, M. Honda, T. Oohashi, K. Shimizu, and M. Senda, "Development of a brain PET system, PET-Hat: A wearable PET system for brain research," *IEEE Trans. Nucl. Sci.*, vol. 58, no. 3, pp. 668–673, Jun. 2011.

[10] M. Bergeron, J. Cadorette, J.-F. Beaudoin, M. D. Lepage, G. Robert, V. Selivanov, M.-A. Tetrault, N. Viscogliosi, J. P. Norenberg, R. Fontaine, and R. Lecomte, "Performance evaluation of the LabPET APD-Based digital PET scanner," *IEEE Trans. Nucl. Sci.*, vol. 56, no. 1, pp. 10–16, Feb. 2009.

[11] J. Kataoka, H. Matsuda, F. Nishikido, M. Koizumi, H. Ikeda, M. Yoshino, T. Miura, S. Tanaka, Y. Ishikawa, N. Kawabata, K. Shimizu, Y. Matsunaga, S. Kishimoto, H. Kubo, Y. Yanagida, and T. Nakamori, "Development of an APD-Based PET module and preliminary resolution performance of an experimental prototype gantry," *IEEE Trans. Nucl. Sci.*, vol. 57, no. 5, pp. 2248–2454, Oct. 2010.

[12] D. P. McElroy, W. Pimpl, B. J. Pichler, M. Rafecas, T. Schuler, and S. I. Ziegler, "Characterization and readout of MADPET-II detector modules: Validation of a unique design concept for high resolution small animal PET," *IEEE Trans. Nucl. Sci.*, vol. 52, no. 1, pp. 199–204, Feb. 2005.

[13] A. Yoshikawa, T. Yanagida, Y. Yokota, K. Kamada, Y. Usuki, S. Yamamoto, M. Miyake, M. Baba, K. Sasaki, T. R. dos Santos, M. Ito, M. Takeda, and N. Ohuchi, *Opt. Mat.*, vol. 32, pp. 1294–1297.

[14] K. Kamada, T. Yanagida, T. Endo, K. Tsutumi, Y. Fujimoto, A. Yoshikawa, J. Pejchal, and M. Nikl, "Composition engineering in Ce doped (Lu, Gd)$_3$(Ga, Al)$_5$O$_{12}$ single crystal scintillators," *Cryst. Growth Des.*, vol. 11, pp. 4484–4490, Aug. 2011.

[15] K. Kamada, T. Yanagida, J. Pejchal, M. Nikl, T. Endo, K. Tsutumi, A. Yoshikawa, J. Pejchal, and M. Nikl, "Scintillator-oriented combinatorial search in Ce-doped (Y, Gd)$_3$(Ga, Al)$_5$O$_{12}$ multicomponent garnet compounds," *J. Phys. D: Appl. Phys.*, vol. 44, pp. 505104–505109, Dec. 2011.

[16] K. Kamada, T. Yanagida, T. Endo, K. Tsutumi, Y. Usuki, M. Nikl, A. Yoshikawa, J. Pejchal, and M. Nikl, "2 inch diameter single crystal growth and scintillation properties of Ce:Gd$_3$Al$_2$Ga$_3$O$_{12}$," *J. Cryst. Growth*, vol. 352, pp. 88–90, Aug. 2012.

[17] A. Yoshikawa, Y. Fujimoto, A. Yamaji, S. Kurosawa, J. Pejchal, M. Sugiyama, S. Wakahara, Y. Futami, Y. Yokota, K. Kamada, K. Yubuta, T. Shishido, and M. Nikl, "Crystal growth and characterization of Ce:Gd$_3$(Ga,Al)$_5$O$_{12}$ single crystal using floating zone method in different O_2 partial pressure," *Opt. Mat.*, vol. 35, pp. 1882–1886, Sep. 2013 [Online]. Available: http://dx.doi.org/10.1016/j.optmat.2013.02.021

[18] P. Prusa, K. Kamada, M. Nikl, A. Yoshikawa, and J. A. Mares, "Light yield of (Lu, Y, Gd)$_3$Al$_2$Ga$_3$O$_{12}$:Ce garnets," *Radiation Measurements*, 2013, doi.org/10.1016/j.radmeas.2013.01.055, in press.

[19] K. Shimazoe, Y. Wang, H. Takahashi, K. Kamada, M. Yoshino, J. Kataoka, Y. Yamaya, T. Yanagida, A. Yoshikawa, and K. Kumagai, "Time over threshold based digital animal PET (TODPET)," in *2011 IEEE Nuclear Science Symp./Medical Imaging Conf. Rec.*, pp. 3267–3271.

Nuclear Instruments and Methods in Physics Research A 731 (2013) 109–113

Contents lists available at ScienceDirect

Nuclear Instruments and Methods in Physics Research A

journal homepage: www.elsevier.com/locate/nima

Time over threshold based multi-channel LuAG-APD PET detector

Kenji Shimazoe [a,*], Tadashi Orita [a], Yasuaki Nakamura [b], Hiroyuki Takahashi [a,b]

[a] Department of Nuclear Engineering and Management, The University of Tokyo, 7-3-1 Hongo, Bunkyo-ku, Tokyo 113-8656, Japan
[b] Department of Bioengineering, The University of Tokyo, 7-3-1 Hongo, Bunkyo-ku, Tokyo 113-8656, Japan

ARTICLE INFO

Available online 11 June 2013

Keywords:
PET
APD
Time over threshold

ABSTRACT

To achieve efficient signal processing, several time-based positron emission tomography (PET) systems using a large number of granulated gamma-ray detectors have recently been proposed. In this work described here, a 144-channel Pr:LuAG avalanche photodiode (APD) PET detector that uses time over threshold (ToT) and pulse train methods was designed and fabricated. The detector is composed of 12 × 12 Pr:LuAG crystals, each of which produces a 2 mm × 2 mm × 10 mm pixel individually coupled to a 12 × 12 APD array, which in turn is connected pixel-by-pixel with one channel of a time over threshold based application-specific integrated circuit (ToT-ASIC) that was designed and fabricated using a 0.25 μm 3.3 V Taiwan Semiconductor Company complementary metal oxide semiconductor (TSMC CMOS) process. The ToT outputs are connected through a field-programmable gate array (FPGA) to a data acquisition (DAQ) system. Three front-end ASIC boards—each incorporating a ToT-ASIC chip, threshold control digital-to-analog converters (DACs), and connectors, and dissipating power at about 230 mW per board—are used to read from the 144-channel LuAG-APD detector. All three boards are connected through an FPGA board that is programmed to calibrate the individual thresholds of the ToT circuits to allow digital multiplexing to form an integrated PET module with a measured timing resolution of 4.2 ns. Images transmitted by this PET system can be successfully acquired through collimation masks. As a further implementation of this technology, an animal PET system consisting of eight gamma pixel modules forming a ring is planned.

1. Introduction

Modern high-resolution positron emission tomography (PET) systems require large numbers of granulated gamma detectors, each of which can resolve hundreds of thousands of pixels within an area of less than 2 mm^2. Many such pixelated detectors utilize an analog multiplexing method (such as Anger logic) to decrease the number of readout channels needed, although individual readout system remains necessary to attain theoretically achievable spatial resolutions [1]. However, individual readout systems require a large number of interconnections, which often leads to wiring problems. Recently, several time-based ASICs with simplified circuit structuring have been investigated for potential use in more compact PET systems [2–8]. Such circuits encode energy and other information (i.e., position and time) into the width of pulses (i.e., pulse width modulation) sent via binary lines to each channel of the readout. In this paper, a time over threshold (ToT)-based compact avalanche photodiode (APD) PET module using granulated gamma detectors and ToT-ASIC technology to produce individual readouts is described. Each channel of the fabricated ToT-ASIC consists of a preamplifier and a comparator that convert input charges into digital pulses with low power dissipation over a small number of digital transmission lines.

2. Front-end time over threshold ASIC

The 48-channel ToT-based ASIC was designed and fabricated to operate as a front-end electronic interface for a 144-channel Pr:LuAG APD pixel array. Each channel of the chip consists of a charge-sensitive preamplifier and a ToT circuit that together generate a digital output. Fig. 1 shows a picture of a ToT-ASIC; the pads of the 48 input channels are located on the left side of the chip, whereas those of the 48 output channels are located on the right side. Pads providing chip bias and threshold adjustment are located on both the upper and lower sides. In the simulation design, the gain of the preamp was set to 5 mV/fC using a 200 fF feedback capacitor to provide readout from the APD detector, resulting in a gain of 50 at a voltage of 380 V. The ASIC chip was fabricated using a 0.25 μm 3.3 V Taiwan Semiconductor Company complementary metal oxide semiconductor (TSMC CMOS) process; this chip has a die size of 2 mm × 5 mm. Three 3 cm × 6 cm front-end readout boards—each consisting of coupling capacitors, a ToT-ASIC with 48 input and 48 output channels apiece, six

* Corresponding author. Tel./fax: +81 3 5841 6974.
E-mail address: shimazoe@it-club.jp (K. Shimazoe).

0168-9002/$ - see front matter © 2013 Elsevier B.V. All rights reserved.
http://dx.doi.org/10.1016/j.nima.2013.05.141

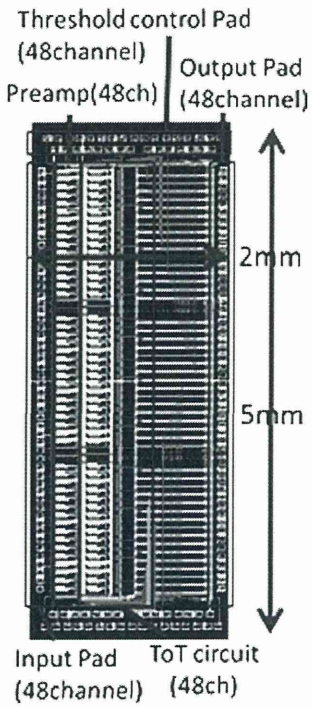

Fig. 1. Design of the 48-channel ToT-ASIC (2 mm × 5 mm).

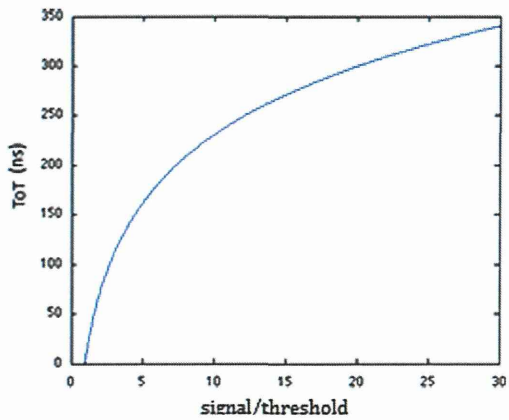

Fig. 2. HSPICE simulation of the relation between signal-to-threshold ratio and ToT (ns).

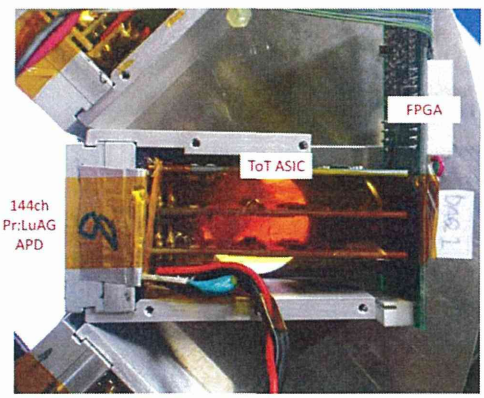

Fig. 3. Photo of 144-channel PET module.

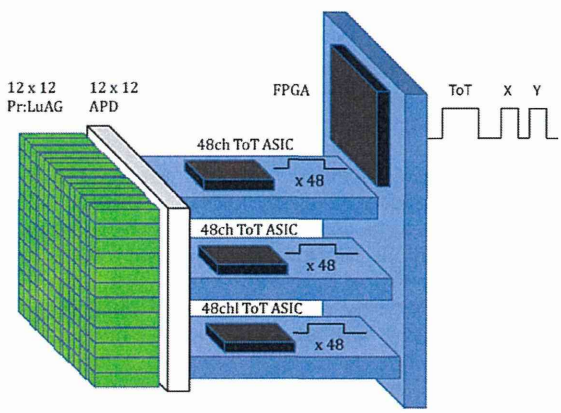

Fig. 4. Design and readout scheme of module using ToT-ASICs to readout the 144-channel gamma pixel detector.

digital-to-analog convertors (DACs), and peripheral components —were used to readout from the 144-channel LuAG-APD detector. Because individual threshold control is important in compensating for the variation between channels in an ASIC, the threshold of each individual channel is adjustable at 12-bit resolution (corresponding to 0.8 mV) by the external DACs. Fig. 2 shows an HSPICE simulation of the relation between the ToT and the signal-to-threshold ratio. The relation appears to be nonlinear, but by using a look-up table based on the linearity curve, the nonlinearity can be calibrated. The ToT output demonstrates this nonlinear relation between energy and output pulse width when a comparator is applied because the preamplifier output is typically composed of a fast rising edge and a slow exponential decay (depending on the feedback resistor and capacitor used). The preamplifier is designed using a normal cascade topology and has a measured RMS noise of 510 electrons at a shaping time of 0.5 μs and a measured rise time of ~12 ns. As a time resolution of 4.2 ns—which is usable within a 10 ns coincidence timing window—was measured for a single PET module, it was judged suitable for use in our proposed PET system.

3. 144-Channel PET detector module and pulse train readout method

Figs. 3–5 show a photograph, design scheme, and block layout, respectively, of the entire module system consisting of 144-channel Pr:LuAG pixel crystals (Furukawa Company) [9], a 144-channel pixel APD (products of Hamamatsu Photonics) [10], three newly developed ToT-ASIC boards, and an integrating field-programmable gate array (FPGA) board (Altera Cyclone II). With a density of 6.7 g/cm^3, an energy resolution of approximately 5% at 662 keV, and a fast decay time (< ~25 ns), Pr:LuAG has characteristics suitable for use in a PET detector. Each pixelated crystal is coupled with one pixel of a UV-enhanced APD (QE= 55% at 310 nm) array using silicone grease (OKEN, 6262A), and all of the APD pixels are connected in turn to the inputs of a ToT-ASIC. Each of the 144-channel outputs from the ToT-ASIC is fed into a FPGA device (Altera Cyclone III) for multiplexing to transmit to the DAQ through a single line. The threshold

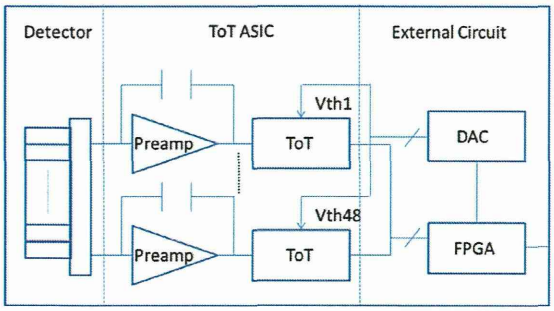

Fig. 5. Block diagram of fabricated 144-channel PET module.

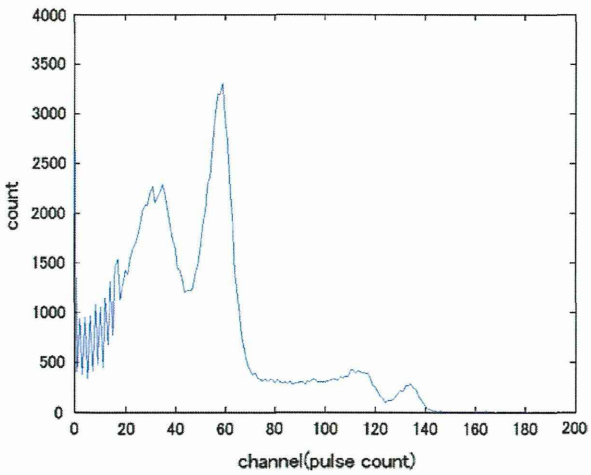

Fig. 6. Energy spectrum from ^{22}Na (pulse width channel on the X-axis versus count on the Y-axis) measured by ToT-ASIC with 250 MHz sampling FPGA. One count equals 4 ns along the X-axis.

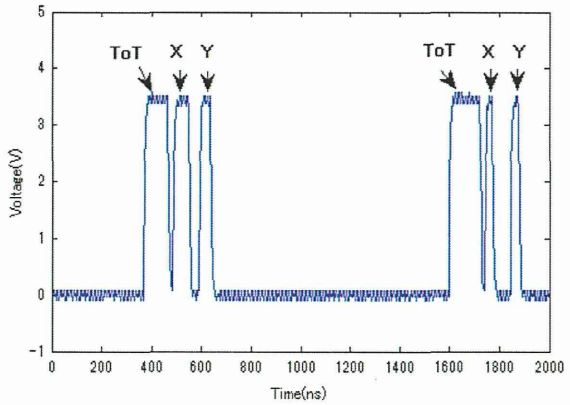

Fig. 7. Oscilloscope image of waveforms of captured pulse trains used to transmit the energy, timing, and position of incident gamma rays.

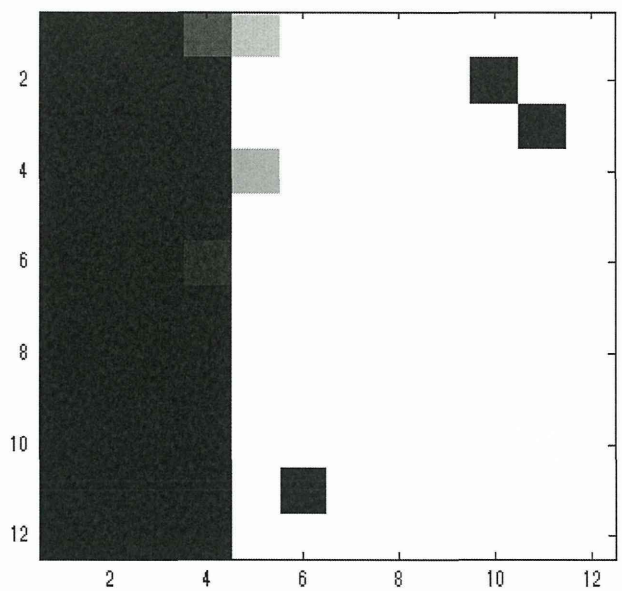

Fig. 8. Reconstructed transmission image with left-half mask.

controlling DACs are also connected to the FPGA. Fig. 6 shows the measured energy spectrum of a typical channel with a ^{22}Na source. At 511 keV and 1.28 MeV, energy resolution from the source is about 10% (@ 511 keV), which meets the requirements for use as a PET detector. The degree of energy resolution is mostly determined by the characteristics of the crystal and APD, although kickback noise from the digital circuit is also present. The observed ToT pulse width varies from 100 to 400 ns, depending on the energy and pulse width measured by the FPGA device (the Altera Cyclone III used here has 250 MHz sampling with a 4 ns period). At approximately 20,000 photons/MeV, the estimated charge produced by the coupled APD and Pr:LuAG detectors at 390 V is between 10 and 50 fC; in this range, the pulse width modulation system has a 7–8 bit digital conversion resolution.

In this system, the pulse train readout method [11] is used to multiplex 144 channels of ToT signals into a single line. Two tags (X and Y) are added following each ToT pulse to specify the position of the incident gamma-ray, and multiple pulses are used to encode the energy and position within a single transmission line. In the experiment conducted for this paper, a time duration unit of 20 ns was used and the X position was expressed using pulses of duration 20–240 ns. The additional pulses were generated by an FPGA (Altera Cyclone II board) with a clock rate of 50 MHz. Fig. 7 shows oscilloscope readings of the waveforms of the captured pulse trains. In this PET system, the leading ToT edge and pulse width are used to derive time information and energy information, respectively.

4. Transmission image and animal PET

Using a 1 MBq ^{22}Na point source, a module employing the pulse train method described above was tested. The module was located a distance of 10 cm from the point source and covered with lead collimation masks of differing patterns. Transmission images obtained using three collimation mask patterns (left-half, bottom-half, and pattern) are shown in Figs. 8–10, respectively. These transmission images were acquired with 30-s exposures, from which the background counts (measured in the absence of a source) were subtracted (the main component of background activity was the internal self-radioactivity of lutetium within the Pr:LuAG crystals). Three dead channels, which can be seen as black points in Fig. 8, resulted from problems with the board implementation process and damage to the ASIC from incident charges.

Improvements will be needed in implementing the next design, but no further damage was observed in the experiment. From Fig. 11, which shows a position map of the detector, it can be seen that the separation shown between the crystals is clearer than in conventional analog-multiplex systems; owing to the use of individual readouts and digital multiplexing, the display appears point-like. Based on this system, an animal PET system with eight 144-channel LuAG-APD PET modules is planned for construction (Fig. 12).

5. Conclusion

In the study described in this paper, a 144-channel pixel gamma-ray detector with an individual readout scheme was fabricated using a 12×12 array of LuAG crystals, a 12×12 UV-enhanced APD array, and three ToT-ASICs. The 2 mm^2 detector pixel size was sufficient to achieve high spatial resolution, and a three-pulse train method to encode energy, time, and position information was used to compress 144 channels into a single transmission line. Although a few dead channels were present,

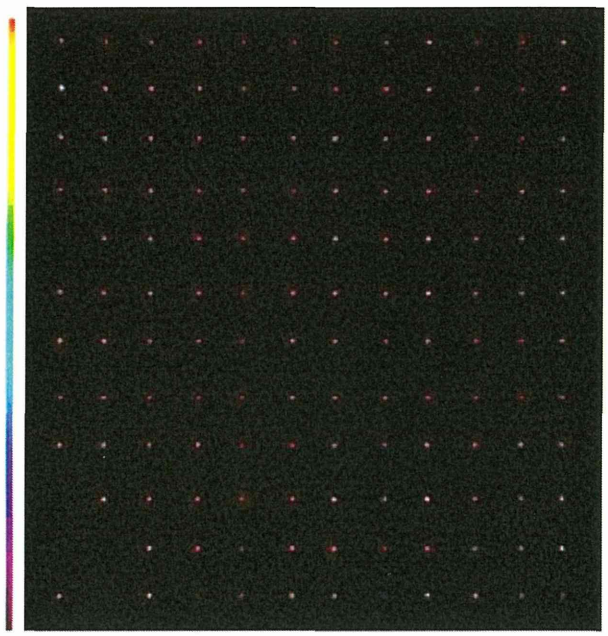

Fig. 11. Position map of the detector.

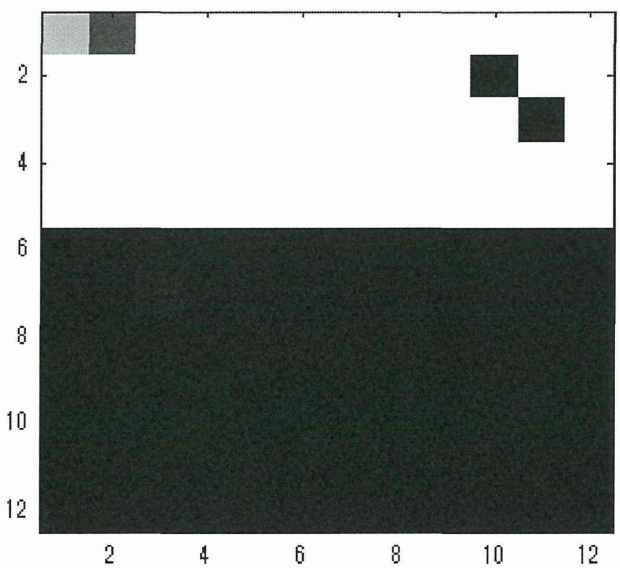

Fig. 9. Reconstructed transmission image with bottom-half mask.

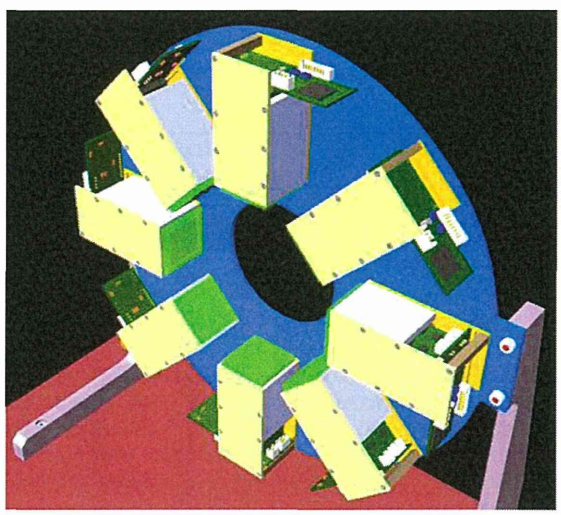

Fig. 12. Planned PET ring consisting of eight APD PET modules.

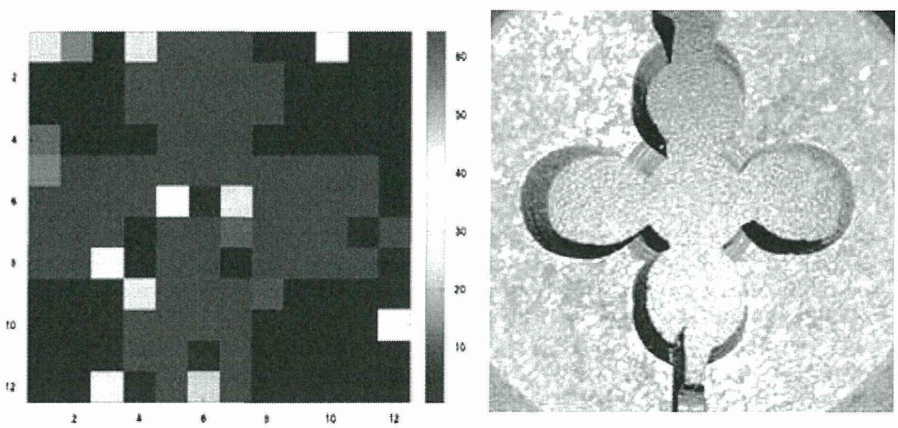

Fig. 10. Reconstructed transmission image with a patterned mask.

several transmission images were successfully acquired. The fabricated system has an energy resolution of 10% and a time resolution of 4 ns, and thus is usable as a PET detector.

Acknowledgment

This study was conducted as a part of the project "R&D of Molecular Imaging Equipment for Malignant Tumor Therapy Support," supported by the New Energy and Industrial Technology Development Organization (NEDO).

References

[1] R. Lecomte, Nuclear Instruments and Methods in Physics Research Section A: Accelerators, Spectrometers, Detectors and Associated Equipment 527 (1–2) (2004) 157 11 July.
[2] K. Shimazoe, Y. Wang, H. Takahashi, K. Kamada, M. Yoshino, J. Kataoka, Y. Yamaya, T. Yanagida, A. Yoshikawa, K. Kumagai, Time over Threshold based digital animal PET (TODPET), in: Proceedings of the IEEE Nuclear Science Symposium and Medical Imaging Conference (NSS/MIC), 2011, pp. 3267–3271.
[3] K. Shimazoe, H. Takahashi, B. Shi, T. Furumiya, J. Ooi, Y. Kumazawa, H. Murayama, IEEE Transactions on Nuclear Science 57 (2) (2010) 782.
[4] Z. Deng, A.K. Lan, S. Xishan, C. Bircher, L. Yinong, S. Yiping, IEEE Transactions on Nuclear Science 58 (6) (2011) 3212, Part: 2.
[5] M. Streun, H. Larue, C. Parl, K. Ziemons, A compact PET detector readout using charge-to-time conversion, in: Proceedings of the 2009 IEEE Nuclear Science Symposium Conference Record (NSS/MIC), 2009, pp. 1868–1870.
[6] C. Parl, H. Larue, M. Streun, K. Ziemons, S. van Waasen, IEEE Transactions on Nuclear Science 59 (5) (2012) 1809, Part: 1.
[7] Peter D. Olcott, Craig S. Levin, Pulse width modulation: a novel readout scheme for high energy photon detection, in: Proceedings of the IEEE Nuclear Science Symposium Conference Record, NSS '08, 2008, pp. 4530–4535.
[8] N. Ollivier-Henry, W. Gao, X. Fang, N.A. Mbow, D. Brasse, B. Humbert, C. Hu-Guo, C. Colledani, Hu. Yann, IEEE Transactions on Biomedical Circuits and Systems 5 (1) (2011) 90.
[9] K. Kamada, T. Yanagida, K. Tsutsumi, Y. Usuki, M. Sato, H. Ogino, A. Novoselov, A. Yoshikawa, M. Kobayashi, S. Sugimoto, F. Saito, IEEE Transactions on Nuclear Science 56 (3) (2009) 570.
[10] J. Kataoka, M. Koizumi, S. Tanaka, H. Ishibashi, T. Nakamori, N. Kawai, H. Ikeda, Y. Ishikawa, N. Kawabata, Y. Matsunaga, S. Kishimoto, H. Kubo, Nuclear Instruments and Methods in Physics Research Section A Accelerators, Spectrometers, Detectors and Associated Equipment 604 (1–2) (2009) 323 1 June.
[11] K. Shimazoe, H. Takahashi, B. Shi, T.; Furumiya, J. Ooi, Y. Kumazawa, Pulse train multiplexing method for pixellated gamma detectors, in: Proceedings of the IEEE Nuclear Science Symposium Conference Record, NSS '08, 2008, pp. 4704–4706.

放 射 線 Vol. 39, No.3 (2014)

放射線計測用ASICの開発

東京大学・工学系研究科　島添 健次

Development of Front-End ASIC for Radiation Detection and Measurement

K. Shimazoe
Department of Nuclear Engineering and Management, The University of Tokyo, Tokyo, 113-8656
e-mail: Shimazoe@bioeng.t.u-tokyo.ac.jp

For realizing the multichannel spectroscopy of gamma rays, the technology of integrated circuits is necessary. Multi-channel gamma ray spectroscopy is very important for many applications including the medical imaging and the environmental monitoring. The current progress in the development of application specific integrated circuit (ASIC) for multi-channel radiation detection is introduced and reviewed.

1. はじめに

近年の高計数率、高分解能の放射線イメージングにおいては、高度にピクセル化された検出器を用いることが必要となってきている。また放射線計測において必要とされる情報はアプリケーションによって様々である。放射線計測において特に考慮されるものとして、時間分解能、エネルギー分解能、計数率、位置分解能、信号波形解析などの要素が存在する。

例えば高空間分解能のPositron Emission Tomography (PET)システムにおいては時間分解能や位置分解能などが重要であり計数率やエネルギー分解能が良好であることが望ましい。一方でコンプトン散乱を利用するコンプトンカメラ方式ではエネルギー分解能や位置分解能などが重要なファクターであり計数率が良好であることが望ましい。また単純にカウントを積算する場合のガンマ線イメージングではエネルギー分解能は必要なく、福島第一原子力発電所事故後の原発内の高線量地域でのモニタリングやイメージングにおいては高い計数率が必要とされることは容易に想像される。一方でこのような要請を突き詰めていくと将来的には高時間分解能、高エネルギー分解能、高計数率、高度波形分析をマルチチャネルにわたって実現することが必要となる。

このような要請をピクセル化によって引き起こされるマルチチャネルに対して実現するためには、消費電力や信頼性の観点から専用の集積回路 (application specific integrated circuit ASIC)の開発や利用が必須となる。ここではこれまでに行なってきた多チャンネルシステムの計数率や分解能などを劣化させないようなASIC技術開発の取り組みについて紹介することとしたい。

2. 放射線検出用ASIC

2.1 ASIC・VLSI設計環境

現在の日本における大学教育研究のおけるASICや large scale integration (LSI)の設計開発の推進は主にVDEC (VLSI Design and Education Center)[1]によって行われている。VDECでは設計に必要なCADツールの提供や試作プロセスの提供を行なっている。例として2013年8月現在, VDECで利用可能な試作プロセスは CMOS 0.8 m (オンセミ-三洋半導体製造社)、CMOS 0.18 m (ローム社)、CMOS 65 nm (eShuttle)などが存在する。CMOS (complementary metal oxide semiconductor)プロセスの微細化はムーアの法則と呼ばれ、主にディジタル回路を中心とした開発に用いられてきた。現在Intel CPU Haswellに主に用いられているプロセスは 22 nm、また並列で可変なディジタル信号処理チップであるAltera社やXilinx社のfield programmable gate array (FPGA)に用いられているプロセスは28 nm TSMC CMOS プロセスである。一方、放射線計測領域で主に用いられているプロセスはおよそ0.35 μm ~ 0.18 μm CMOSであり、90 nmや65 nmの研究が活発に行われている。動作電圧は現在3.3 Vや2.5 Vが主流となりつつあるが今後1.2 Vや1 V以下へ進んでいくと考えられている。ASICの設計においてはSPICEによる回路シミュレーションからレイアウト設計、デザインルールチェックなどに加えてディジタルの場合は論理合成から配置配線までを行うことになる。CMOSプロセスはアナログ・ディジタル混載システムを構築するためには最適のプロセスと言える。

放射線計測においては、検出器からの微弱信号を電圧に変換する電荷感応増幅器 (Charge Sensitive Amplifier

平成25年8月12日受付・受理 Received and accepted 12th, August, 2013

CSA)や波形整形回路 (Shaping Amplifier SA)、後段のAnalog Digital Converter (ADC)などが主な構成要素となる。多チャンネル化においては各チャネルに CSA～ADCまでを搭載できることが望ましいが、現実的にはADCの消費電力の高さやダイ面積の制限などから困難であり、ADCの前段でアナログ手法によりマルチプレクスを行う手法が取られる事が多い。一方でマルチプレクスを行うことで計数率の劣化が起こると主に手法によっては、ノイズ増加の原因ともなり最終的なシステムの性能の制約となってきた[2)3)4)]。本稿では上記の問題を解決する試みとして、各チャネルに対して並列でディジタル変換を行う方式を採用し、PETや他の放射線計測用に試作、開発をおこなったASICについて紹介することとしたい。

2.2 波形サンプリング型ASIC

波形サンプリング型ASIC[5)]は放射線計測に必要なすべてのフロントエンド回路を1チャネルに含んだマルチチャネルチップである。各チャネルに電荷感応増幅器、ゲイン可変増幅器、フラッシュADCを搭載し1チップで入力信号波形をリアルタイムにディジタル変換を行う(Fig. 1参照)。1チップ、検出器近傍でディジタル変換を行うため、フロントエンドから外部のデータ取得系までのデータ転送において信号の劣化が起こることはない。

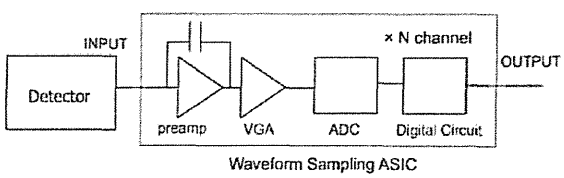

Fig. 1 Basic structure of Waveform Sampling ASIC, which consists of a charge sensitive amplifier, a variable gain amplifier, a free-running ADC and digital circuits.

本チップではフリーランニングADCの搭載により検出器からの信号を1チップでディジタル化し波形分析も可能にすることを目的としている。そのためADCの速度は100 MHz以上で動作させるように設定している。PETでの用途ではnsオーダーの時間分解能を実現するために高速のサンプリングが必要である。一方で各チャネルにADCをもたせるため、消費電力やチップダイサイズなどの制約からビット数は6 bitとした。通常フラッシュADCでは2^6個のコンパレータ素子が必要となるが、フォールディングADC構成をとること (Fig. 2)で低消費電力、ダイサイズの低減を図っている。

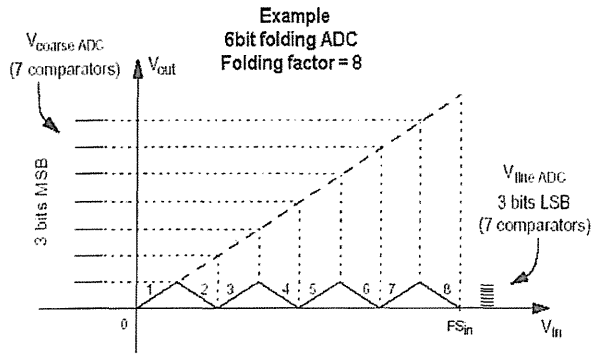

Fig. 2 The principle of folding ADC to reduce the power dissipation and the number of comparators

電荷感応増幅器は高速化、高ゲイン化のためテレスコーピックカスコード型の増幅器を用いた (Fig. 3)。Fig. 4に波形整形時間に対するequivalent noise charge (ENC) の値を示す。0.5μsの整形時定数時に880電子 (FWHM)が観察された。PET用としては十分な性能を有していることが確認できている。

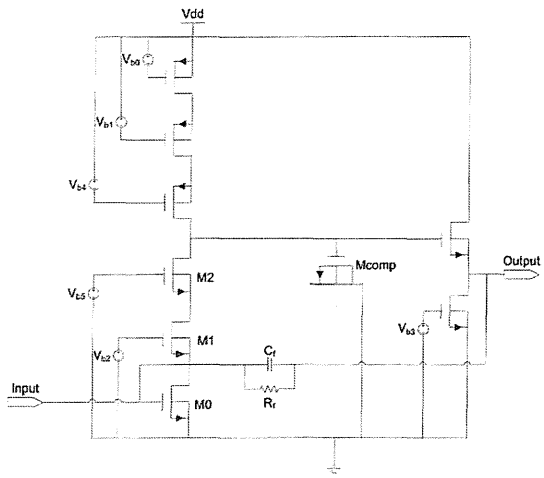

Fig. 3 Schematic of the telescopic cascode preamplifier

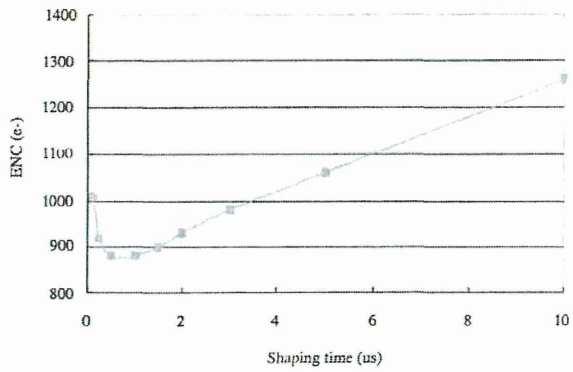

Fig. 4 Measured equivalent noise charge (ENC) in telescopic cascode preamplifier

実際の設計においては、電荷感応増幅器からADCまでの設計はHSPICEおよびレイアウトを用いた手動設計により行なっているが、マルチプレクスやfirst in first out (FIFO) 機能などはハードウェア記述言語 Verilog-HDL によりコーディングを行い、論理合成およびアナログ・ディジタル混載チップの配置配線を行うことで試作設計を進めている。

Fig. 5に作成したチップのレイアウトおよびパッケージ写真を示す。ダイサイズは4.9 mm角となっており図のレイアウトの左側が入力、右側がディジタル出力となっている。チップレイアウトの大半を100 MHz 6 bitの ADCおよびディジタル回路が占めている事がわかる。チップはROHM社の0.35 μm / 3.3 V CMOSプロセスを用いて試作を行った。消費電力はおよそ2W @ 50MHzであった。

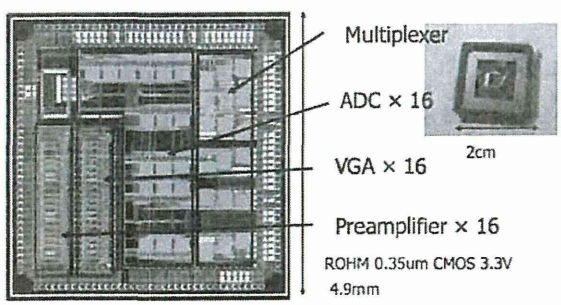

Fig. 5 Layout picture of the fabricated die including 16 channels of waveform sampling function and its package

波形サンプリング型ASICは出力されたディジタル波形を用いて波形信号を解析することが可能である。特に近年ではFPGAの発展が目覚ましく、今後も動作周波数の高速化が進むと考えられるため後段の信号処理システムとの相性もよい。Fig. 6に異なる立ち上がり時間を持つ信号にたいする応答を示す。ディジタル化された信号においても異なる立ち上がり時間が再現されていることがわかる。PETなどのアプリケーションにおいては結晶内の深さ情報depth of interaction (DOI)を得るために異なる濃度の不純物を添加した複数種類のシンチレータを用いることが行われている。例えばGSO結晶においてはCe濃度を0.5 mol%から1.5 mol%まで変化させることで時定数を15 nsから 60 nsまで変化させることが可能である。波形弁別により異なる発光時定数をもつ結晶を分離することでDOI情報を得ることができる。

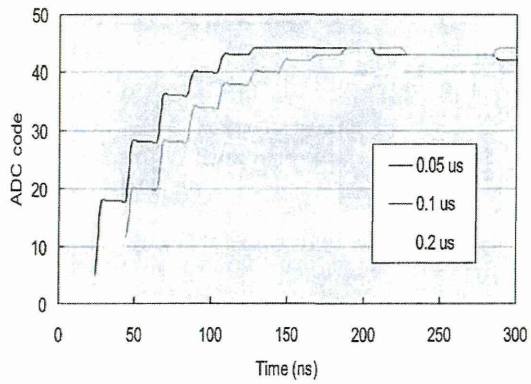

Fig. 6 Example of digitized waveforms for 3 input pulses with different rise time (0.05 μs, 0.2 μs and 0.2 μs) by the developed waveform sampling ASIC.

2.3 時間幅信号処理ASIC

従来のスペクトロスコピーシステムにおいては、初段に電荷感応増幅器を用いて、エネルギー情報を電圧値に変換し、波高値を計測するためコンパレータを配列したADCが必要となる(波高値計測システム)。一方でコンパレータを1つのみ用いることで、入力信号をディジタル信号に変換し、パルスの幅を計測する手法(time over threshold ToT)が簡易的なエネルギー計測の分野で使われてきた(パルス幅計測システム)[6]。ToT方式を用いる利点はコンパレータが各チャネルに対して1つのみであるため大幅な低消費電力化が可能であるということまた1チャネルに対して1ビットの伝送ラインのみが必要であるため多チャンネルシステムに向いているという特性を有している。ToT方式ではエネルギー情報をえることができるためカウンター型の方法と比較しても高度なシステムにも利用可能である (Fig. 7参照)。また本稿で

は従来のToT方式を改良し、高精度エネルギー情報が取得可能なdynamic ToT方式についても紹介する。

特に近年のPET用の検出器では10万チャンネルを超える数の信号処理が必要であり今後時間幅を用いた信号処理システムが重要となってくると考えられる[7]。時間幅を用いた方式はスタンフォード大学のグループやドイツ、中国などのグループでも研究が開始されている[8)9)10)]。

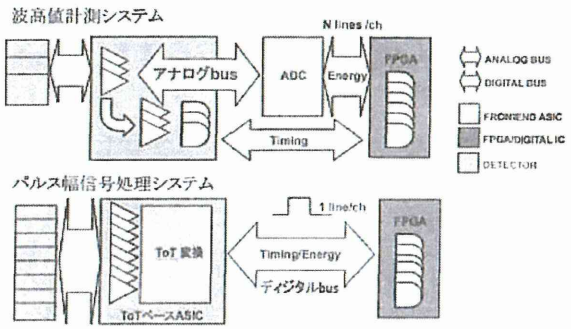

Fig. 7 The comparison of 'pulse height measurement ' and 'pulse width measurement '.

一般的なToT方式の信号処理回路は電荷感応増幅器、波形整形回路、コンパレータで構成される。コンパレータで出力されたディジタル信号のパルス幅を計測することで入射したエネルギーを推定することが可能である。パルス幅のカウントはディジタルパルスなので非常に単純であり、ある周波数クロックを用いてパルスが立ち上がっている時間をカウントするだけでよい。エネルギー計測の分解能は高速のクロックを用いれば用いるほど増加することになる。後段のエネルギー、時間計測システムはパラレル化が非常に簡単である。後段のカウントシステムはFPGAを用いて構成されることが多くGHzで動作するデバイスも出てきているため今後の高分解能化もすすむと考えられる。

Fig. 8に典型的な入力電荷に対するToT応答を示す。この例では20 fCに対して120 ns, 60 fCに対して240 n程度の出力幅が得られている。250 MHz (1unit = 4 ns)のパルスカウントクロックを使うことで6 bit程度の分解能を実現可能である。また1 GHz, 4GHz であればそれぞれ8 bit, 10 bitの分解能が得られる。また一方で図からわかるように通常のToT方式では入力電荷と出力ToTの幅の関係は非線形であり最終的なアプリケーションによってはルックアップテーブルを用いた補正が必要となる。我々のグループではコンパレータの動的な閾値を用いて回路レベルで線形性の補正を行う方式 (dTOT)を提案しておりこれについては後述する。

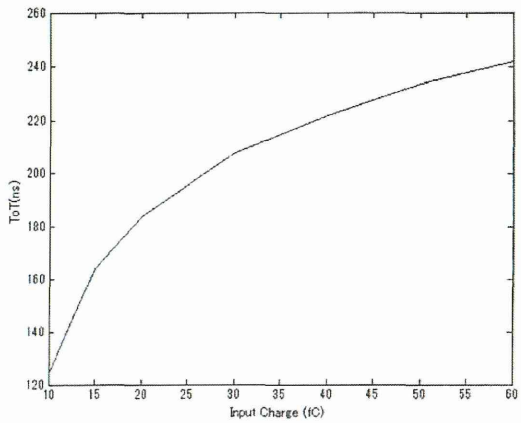

Fig. 8 Example of the response of ToT (input charge versus pulse width)

一方で10万チャネルを超えるようなシステムでは1チャネルに対して1ビットであっても後段の信号処理が対応不可能な場合が存在する。ToTシステムではフロントエンドでディジタル化されるため、ToT回路の後段にディジタル回路を追加することでマルチプレクスも比較的容易に（ディジタル回路的に）行うことが可能である。例えばToTの出力をwired-ORで接続しToTパルスの後続に位置情報をコードしたパルスをディジタル的に発生させる（パルストレイン方式）ことで、容易にマルチプレクスを実現することができる (Fig. 9)。

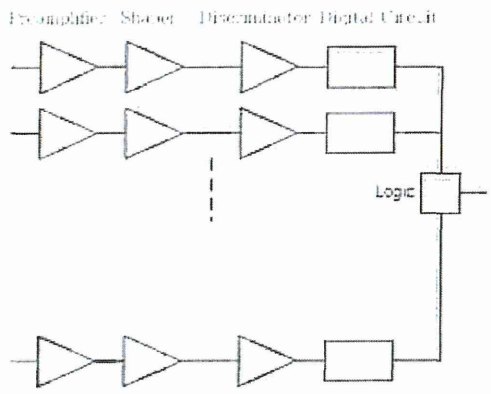

Fig. 9 ToT circuits and digital circuits

Fig. 10に開発した12チャネルパルストレイン方式ASICのチップをしめす。左から電荷感応アンプ、CR-RC波形整形増幅器、ウインドウ型コンパレータ、マルチプレクス（パルス列生成）用のディジタル回路が搭載されている。図の右側に見える黄色の３つのパッドがディジタル

出入力（クロック、リセット、1ビット出力）ピンに対応している。Fig. $にASICの出力をキャプチャした波形を示す。長いToTパルスの後にチャネルに対応したパルス列が生成されていることが確認できる(Fig. 11)。後段のFPGAではパルス列の時間幅を計測することで位置情報を特定する。消費電力は50 MHzの動作周波数でおよそ132 mWである。チップはROHM社CMOS 0.35 μm 3.3Vプロセスを使用した。

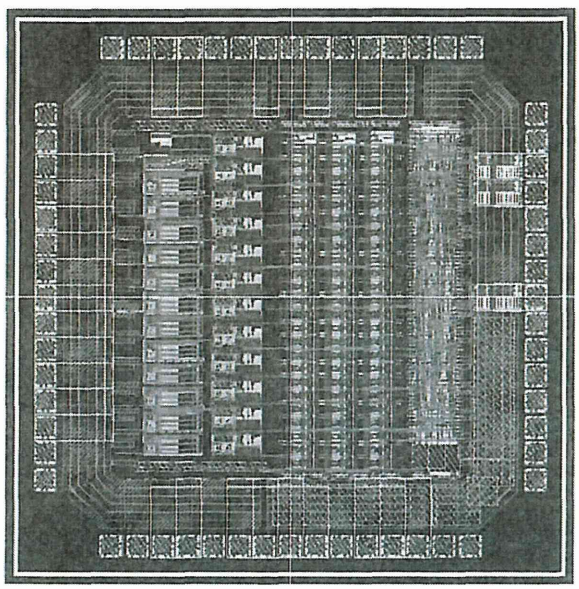

Fig. 10 Layout of pulse train ASIC including 8 channels in a die of 2.5 mm x 2.5 mm, one channel includes a charge sensitive preamplifier, CR-RC shaping amplifier and comparators and digital circuits.

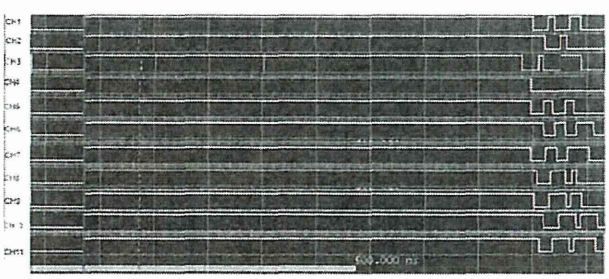

Fig. 11 The output waveforms from 'Pulse Train ASIC'

2.4 エネルギー弁別型時間幅信号処理ASIC

上記で述べたようにToTはマルチチャネルシステムに適した信号処理方法であるが、入力電荷とパルス幅の非線形性からエネルギー分析には補助的にしか用いられて来なかった。ToTの非線形をもたらしているのは入力信号の波形と閾値の関係である。Fig. 8でみたように通常のToTでは信号が大きくなればなるほど飽和領域にはいり同じパルス幅を出力するようになる。

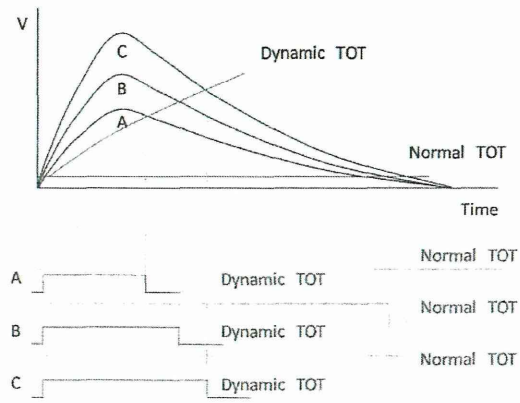

Fig. 12 concept of dynamic time over threshold method for improving the linearity

これを改善するためには入力波形の関数から線形な応答が得られるような関数をもつ動的に変化する閾値を発生させることが必要である。Fig. 12にdynamic ToT手法の概念を示す[11]。例えば一般的にCR-RC波形整形後の信号Vin(t)は理想的には式(1)で示される。

$$\mathrm{Vin}(t) = \mathrm{E}\left(\frac{t}{\mathrm{T}}\right)\mathrm{e}^{-\frac{t}{\mathrm{T}}} \tag{1}$$

ここでEは入力エネルギー、TはCR-RCの時定数である。これに対して、

$$\mathrm{Vth}(t) = \mathrm{A}\left(\frac{t}{\mathrm{T}}\right)^{2}\mathrm{e}^{-t/T} \tag{2}$$

式（2）で表されるような動的閾値関数Vthを生成すれば(ここでAは定数)

2つのコンパレータに対する入力の関係から

$$\frac{t}{T} = \frac{\mathrm{E}}{\mathrm{A}} \tag{3}$$

式(3)で表されるようなパルス幅とエネルギーの線形な関係を得ることが理想的には可能である。またこれまでの研究からCR-RC波形整形入力にたいしては単純なRC回路を用いて生成した閾値関数(式4)

$$\mathrm{Vth}(t) = \mathrm{Vm}\left(1 - \mathrm{e}^{-\frac{t-T}{\mathrm{T}}}\right) \tag{4}$$

を用いることでINL (integrated non linearity) =2.2 %程度を実現できることをシミュレーションにより確かめられている。実際には初期の閾値オフセットやディレイタイムなどの因子が存在するが、時定数を適切に選ぶことで大幅な線形性の改善が可能である。このdynamic ToT方式は回路レベルではコンパレータの出力をコンパレータの閾値関数にモノステーブルマルチバイブレータおよびRC回路を通して帰還させる(Fig. 13)ことで比較的単純に実現が可能であり消費電力もToT方式とほぼ同等である。

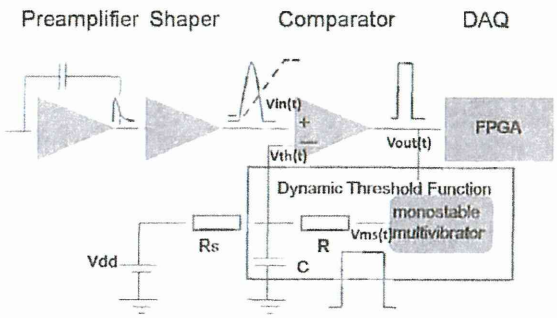

Fig. 12 Block diagram of dynamic ToT method

dToT方式とPHA方式で取得したPr:LuAG-APD検出器のスペクトルの比較をFig. 14に示す。初期閾値の関係で低エネルギー側に非線形性が残るが^{22}Naに対して511 KeVおよび1.28 MeVのエネルギーピークが確認できている。

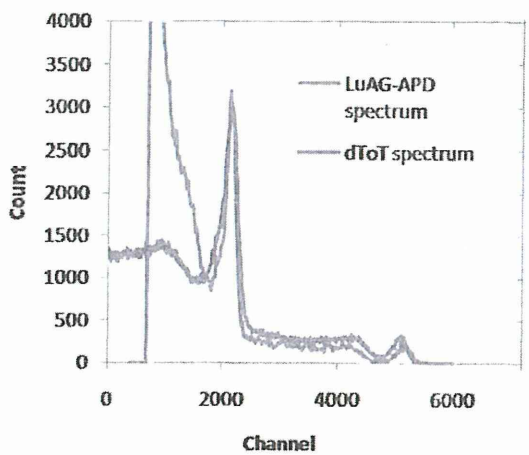

Fig. 14 comparison of two spectra for ^{22}Na source with PHA and dToT method.

我々のグループでは本方式を採用した8チャネルのdToT ASICの試作を行なっている (Fig. 15参照)。 チップサイズは2.5 mm角でありADC搭載型のASICと比較しても小型化が実現できていることがわかる。また消費電力は100 mW以下である。用いたプロセスはTSMC CMOS 0.25 μm 2.5 Vプロセスである。本ASICを用いて線形性を改善したスペクトルを得ることに成功しており今後マルチチャネルのスペクトロスコピーシステムへの適用を目指しており、ヘリ搭載型のコンプトンカメラなどの開発を行なっている。これについては稿を改めて紹介することとしたい。

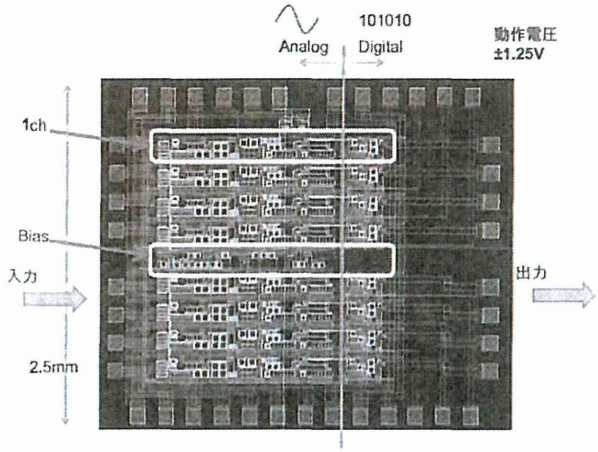

Fig. 15 Layout of 8 channel dynamic ToT ASIC

3. 放射線計測ASICの応用例

2.1 Positron Emission Tomography

高分解能ガンマ線イメージングが必要とされる分野として分子イメージング法として重要なPETがある。PETシステムにおける空間分解能は結晶サイズおよび信号読みだし方式などで決定されることが知られており、多チャンネル化およびピクセルからの個別信号読み出しが望ましい。我々のグループではこれを実現するため低消費電力を実現可能なToT方式を用いたPET用のASICを開発し、Pr:LuAG結晶アレイ、APDアレイと組み合わせることにより世界初ToT方式の純国産高分解能のディジタルPETモジュールの開発をおこなった[12] (Fig. 16参照)。モジュールとしては時間分解能 4 nsエネルギー分解能 10 % @ 511 keVが得られている。モジュールは144チャネルのPr:LuAGのピクセルアレイ（結晶サイズ 2 mm×2 mm× 10mm, 12列×12列)、144チャネルのAPDアレイ(12列×12列)、48チャネルのToT ASIC (チップサイズ 2 mm×5 mm)が3枚およびToT-ASICからの個別読み出しディジタル信号を処理するFPGA(Altera Cyclone

II)から構成される。モジュールとしての消費電力はおよそ600 mW、ASICは0.25 μm 3.3V CMOSプロセスを用いて設計作成した。

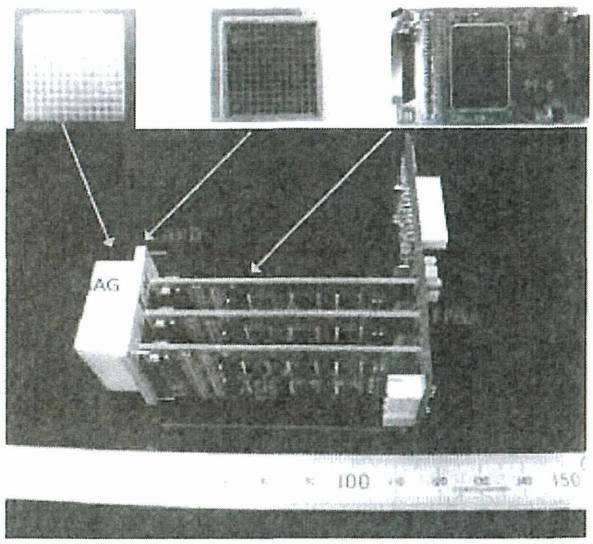

Fig. 16 Time over threshold based PET module with 144 channel digital outputs

また開発したPETモジュールを8個用いて小型のPETシステムを構築した (Fig. 17)。本小型PETシステムを用いて^{22}Na点線源の撮像を行いイメージの再構成に成功し、初期的なデータとして1.76 mm (FWHM)の空間分解能、ML-EM再構成手法により現時点で1.17 mmの空間分解能が得られている[14] (Fig. 18)。

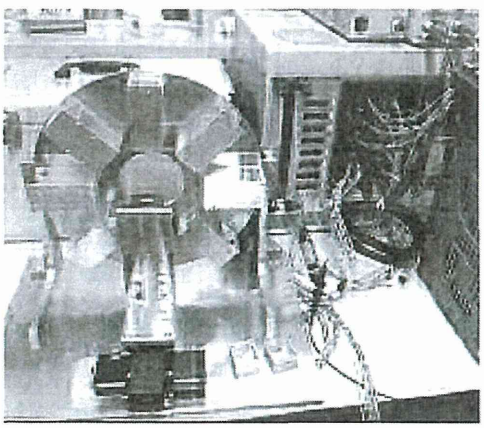

Fig. 17 Small animal PET system using eight developed ToT PET detectors

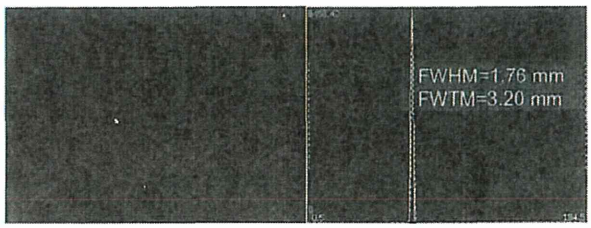

Fig. 18 The acquired image of a ^{22}Na point source using the developed PET system. The point source is clearly illustrated and its resolution is ~ 1.76 mm.

2.2 ガンマカメラシステム

2011年3月に起きた福島第一原子力発電所事故により放射性物質が広範囲に拡散された。現在線量増加に寄与しているのは^{137}Csおよび^{134}Csであり、これらの放射性物質の継続的なモニタリングが必要とされている。また除染を行う前後の効果測定などの要望から、高精度なガンマ線イメージングシステムの開発が望まれている。現在いくつかのグループでガンマカメラやコンプトンカメラなどの開発が進められているが、いずれもマルチチャンネルのガンマ線検出器が主要な技術となっている。ここではPET検出器を応用したピンホールカメラについて紹介する。検出器はバックグラウンドが少なく、発光量の高いCe:GAGG結晶(2 mm×2 mm×6 mm)の12列×12列アレイ検出器を用い、後段はPETモジュールと同じ構造を用いた。それぞれASICやHVへの電源等はUSBの電源経由で作成した。Fig. $に検出器と検出器の前面に設置したピンホールコリメーターの写真を示す (Fig. 19)。コリメーターの穴径は2.5 mmとした。

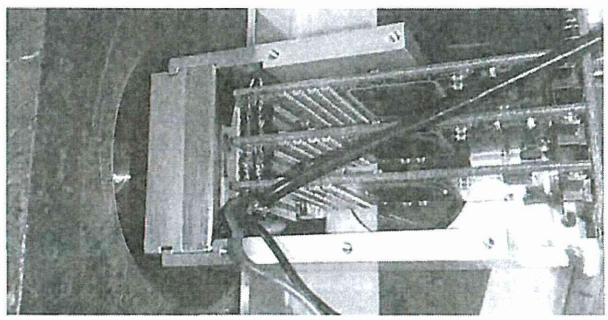

Fig. 19 A pinhole collimator and a gamma detector for gamma ray environmental survey system. The collimator is made of lead.

検出器周りの遮蔽およびピンホールコリメータの厚さは5 cmとし、鉛を用いた。今回作成したピンホールガンマカメラの視野角はおよそ31度である。本検出器をもちいてコリメーター表面より30 cmのところに配置した

^{137}Cs線源 (5 mm× 5 mm× 10 mm)を2個近接した状態と離した状態での撮像を行った。Fig. に取得した画像を示す。2つの線源が分離できていることが確認できた(Fig. 20)。分解能は30 cm先でおよそ24 mm (FWHM)である。今後福島周辺での適用を進めていく予定である。

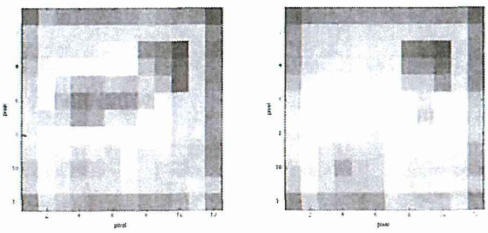

Fig. 20 Image of two ^{137}Cs sources (5 mm×5 mm× 10mm) at the distance of 30 cm from the detector surface.

4. まとめ

現在までにシンチレータや光検出器、半導体検出器の微細加工技術と相まって放射線計測用のASICの開発が進められてきた。2011年3月に起きた福島第一原子力発電所事故後に拡散された放射性物質の可視化の重要性や分子イメージングなどの進展において高精度なガンマ線イメージングへの要請が非常に高まっている。近年増幅度が高い特性の良好な光検出器や結晶の開発が進んでおり、後段の信号処理系との融合が進むことで新たなデバイスの開発が進むことが考えられる。我々のグループでも現在高分解能PET検出器やガンマカメラ、環境モニタリング用のコンプトンカメラなどの研究を進めている。

参考文献

1) 東京大学VDEC http://www.vdec.u-tokyo.ac.jp

2) Herrero-Bosch, V.; Colom, R.J.; Gadea, R.; Espinosa, J.; Monzo, J.M.; Esteve, R.; Sebastia, A.; Lerche, C.W.; Benlloch, J.M., "PESIC: An Integrated Front-End for PET Applications," Nuclear Science, IEEE Transactions on , vol.55, no.1, pp.27,33, Feb. 2008

3) Swann, B.K.; Rochelle, J.M.; Binkley, D.M.; Puckett, B. S.; Blalock, B.J.; Terry, S.C.; Moyers, J. C.; Young, J.W.; Casey, M.E.; Musrock, M. S.; Breeding, J. E., "A custom mixed-signal CMOS integrated circuit for high performance PET tomograph front-end applications," Nuclear Science, IEEE Transactions on , vol.50, no.4, pp.909,914, Aug. 2003

4) Shi, B.; Shimazoe, K.; Wang, Y.; Fujiwara, T.; Takahashi, H.; Iyomoto, N., "Development of Waveform Multiplexing Method With Decay Time Modulation for Front-End ASIC of Pixelated Detectors," Nuclear Science, IEEE Transactions on , vol.58, no.4, pp.2019,2023, Aug. 2011

5) K. Shimazoe, H. Takahashi, J.Y. Yeom, T. Furumiya, J. Ohi, Multi-channel Waveform Sampling ASIC for radiation detection and measurement, Radiation Measurements, Volume 55, August 2013, Pages 87-89

6) Kipnis, I.; Collins, T.; DeWitt, J.; Dow, S.; Frey, A.; Grillo, A.; Johnson, R.; Kroeger, W.; Leona, A.; Luo, L.; Mandelli, E.; Manfredi, P.F.; Melani, M.; Momayezi, M.; Morsani, F.; Nyman, M.; Pedrali-Noy, M.; Poplevin, P.; Spencer, E.; Re, V.; Roe, N.; , "A time-over-threshold machine: the readout integrated circuit for the BABAR Silicon Vertex Tracker," Nuclear Science, IEEE Transactions on , vol.44, no.3, pp.289-297, Jun 1997

7) Shimazoe, K.; Takahashi, H.; Shi, B.; Furumiya, T.; Ooi, J.; Kumazawa, Y.; Murayama, H.; "Novel Front-End Pulse Processing Scheme for PET System Based on Pulse Width Modulation and Pulse Train Method," IEEE Trans. Nucl. Sci., vol.57, no.2, pp.782-786, Apr. 2010

8) Zhi Deng; Lan, A.K.; Xishan Sun; Bircher, C.; Yinong Liu; Yiping Shao, "Development of an Eight-Channel Time-Based Readout ASIC for PET Applications," Nuclear Science, IEEE Transactions on , vol.58, no.6, pp.3212,3218, Dec. 2011

9) Olcott, P.D.; Levin, C.S., "Pulse width modulation: A novel readout scheme for high energy photon detection,"Nuclear Science Symposium Conference Record, 2008. NSS '08. IEEE , vol., no., pp.4530,4535, 19-25 Oct. 2008

10) Parl, C.; Larue, H.; Streun, M.; Ziemons, K.; Van Waasen, S., "Fast Charge to Pulse Width Converter for Monolith PET Detector," Nuclear Science, IEEE Transactions on , vol.59, no.5, pp.1809,1814, Oct. 2012

11) Shimazoe, K.; Takahashi, H.; Boxuan Shi; Orita, T.; Furumiya, T.; Ooi, J.; Kumazawa, Y., "Dynamic Time Over Threshold Method," Nuclear Science, IEEE Transactions on , vol.59, no.6, pp.3213,3217, Dec. 2012

12) Kenji Shimazoe, Tadashi Orita, Yasuaki Nakamura, Hiroyuki Takahashi, Time over threshold based multi-channel LuAG-APD PET detector, Nuclear

Instruments and Methods in Physics Research Section A: Accelerators, Spectrometers, Detectors and Associated Equipment, Available online 11 June 2013, ISSN 0168-9002

13) Lecomte, R.; "Technology Challenges in Small Animal PET Imaging," Nucl. Instrum. Meth. Phys. Res. A, vol.527, no.1-2, pp.157-165, Jul. 2004

14) Shimazoe, K.; Wang, Y.; Takahashi, H.; Kamada, K.; Yoshino, M.; Kataoka, J.; Yamaya, Y.; Yanagida, T.; Yoshikawa, A.; Kumagai, K., "Time over Threshold based digital animal PET (TODPET)," Nuclear Science Symposium and Medical Imaging Conference (NSS/MIC), 2011 IEEE , vol., no., pp.3267,3271, 23-29 Oct. 2011

Czochralski Growth and Scintillation Properties of Ce : $(Gd, Y, Lu)_3 (Al, Ga)_5O_{12}$ Single Crystals

Kei Kamada, Petr Prusa, Martin Nikl, Karel Blazek, Takanori Endo, Kousuke Tsutsumi, Shunsuke Kurosawa, Yuui Yokota, and Akira Yoshikawa

Abstract—1-inch size Ce1%:$Gd_2Lu_1Al_2Ga_3O_{12}$, $Gd_1Lu_2Al_2Ga_3O_{12}$, $Gd_1Y_2Al_{1.5}Ga_{3.5}O_{12}$ and $Lu_2Y_1Al_2Ga_3O_{12}$ **were grown by the Czhocralski (Cz) method. The EPMA techniques is employed to check their chemical composition. Luminescence and scintillation properties were also evaluated. The Ce1%:$Gd_1Y_2Al_2Ga_3O_{12}$ sample showed the highest light yield of around 40 000 photon/MeV. The scintillation decay time was 46.6 ns(63%) and 157 ns(37%).**

Index Terms—**Oxides, scintillator materials, scintillators, single crystal growth.**

I. Introduction

After a decade of R&D of the $Lu_3Al_5O_{12}$-based single crystal scintillators, new material concept was defined, based on multicomponent $(Gd, RE)_3$ $(Ga, Al)_5O_{12}$ host, Re = Lu, Y. Doped by Ce^{3+}, the Gd- and Ga rich host compositions showed amazingly high light yield up to almost 50 000 phot/MeV [1]–[7] which is the value exceeding by 30-40% the best LYSO:Ce materials ever seen. Thanks to the flexibility, cost-effective character and speed of micro-pulling-down method, such a combinatorial study could be done at a number of single crystal samples which is preferable with respect to attempts usually done with powders. Discovery of these ultra-efficient scintillators is based on several previous findings, namely: 1) scintillators based on aluminum garnets show high intrinsic scintillator efficiency, but their figure-of-merit is strongly degraded by shallow electron traps which delay an energy delivery to emission centers [89]; 2) the Ga-admixture into the aluminum garnet effectively diminishes the trapping effects mentioned in 1) [10], but at the same time, the bottom of the conduction band becomes close to the $5d_1$ level of Ce^{3+} which leads to the unwanted excited state ionization of emission centre and light yield decrease [11]; 3) the definition of strategy of the band-gap engineering in the family of aluminum-based garnets [12] and positioning of the $5d_1$ level by crystal field manipulation through the RE site symmetry [13]; 4) the simultaneous admixture of Gd and Ga into the YAG structure leads to dramatic LY increase in Ce : $(Gd\text{-}Y)_3$ $(Al\text{-}Ga)_5O_{12}$ ceramics [14].

In this report, Ce : $(Gd, Lu, Y)_3(Al, Ga)_5O_{12}$ single crystals were grown by the Czochralski (Cz) method. Segregation coefficients of Ce in grown crystals were investigated. Luminescence and scintillation properties such as light yield, non-proportionality, temperature dependence of light yield and decay time were also investigated.

II. Materials and Methods

1) Crystal Growth: Stoichiometric mixtures of 4 N CeO_2, Gd_2O_3, Y_2O_3, Lu_2O_3, β-Ga_2O_3 and α-Al_2O_3 powders (High Purity Chemicals Co.) were used as starting material. Ce : $(Gd, Lu, Y)_3(Al, Ga)_5O_{12}$ single crystals were grown by means of the Cz method using an RF heating system. The rotation rate was 4–12 rpm and the growth rate was 1.0 mm/h. An automatic diameter control system using crystal weighing was applied to control the growth parameters. Crystals were grown from a 50 mm diameter Ir crucible under Ar with adding 30% of CO_2 atmosphere to prevent evaporation of gallium oxide. The seed crystal was a [100] oriented LuAG crystal. After the completion of the crystal growth, the crystal was removed from the melt and was gradually cooled down to room temperature.

2) Gamma-Ray Response Measurement Procedure: Sample pieces with dimensions of 5 × 5 × 1 × mm were cut from the grown single crystal; all surfaces were mechanically polished. Light yield measurement was performed by using an avalanche photodiode (APD) (Hamamatsu, S8664-55). The light yield (LY) of the sample was calibrated from the ^{55}Fe direct irradiation peak to APD.

Non-proportionality was determined by amplitude spectroscopy of scintillation response induced by gamma rays

Manuscript received May 24, 2013; revised July 30, 2013; accepted August 23, 2013. Date of publication January 09, 2014; date of current version February 06, 2014. This work was supported in part by the funding program for next generation world-leading researchers, JSPS, in part by Development of Systems and Technology for Advanced Measurement and Analysis, Japan Science and Technology Agency (JST), in part by Adaptable & Seamless Technology Transfer Program through Target-driven R&D (A-STEP), JST, in part by Japan Society for the Promotion of Science (JSPS) Grant-in-Aid for Exploratory Research (A.Y), in part by JSPS Research Fellowships for Young Scientists (S. Kurosawa), and in part by the Health Labour Sciences Research Grant, The Ministry of Health Labour and Welfare.

K. Kamada is with New Industry Creation Hatchery Center (NICHe), Tohoku University, Sendai, Miyagi 980-8579, Japan, and also with C&A Corporation, T-Biz, Sendai, Miyagi 980-8579, Japan (e-mail: kamada@imr.tohoku.ac.jp).

P. Prusa, M. Nikl and K. Blazek are with Institute of Physics, 162 53 Prague, Czech Republic.

T. Endo and K. Tsutsumii are with Materials Research Laboratory, Furukawa Co. Ltd., Tsukuba, 305-0856, Japan.

S. Kurosawa is with Institute for Material Research, Tohoku University, 980-8577 Sendai, Japan.

Y. Yokota is with New Industry Creation Hatchery Center (NICHe), Tohoku University, Sendai, Miyagi 980-8579, Japan.

A. Yoshikawa is with New Industry Creation Hatchery Center (NICHe) Tohoku University, Sendai, Miyagi 980-8579, Japan; with the C&A Corporation, T-Biz, Sendai, Miyagi 980-8579, Japan; and also with the Institute for Material Reseach, Tohoku University, 980-8577 Sendai, Japan.

Color versions of one or more of the figures in this paper are available online at http://ieeexplore.ieee.org.

Digital Object Identifier 10.1109/TNS.2013.2285613

(Mares *et al.*, 2007). Scintillation crystal is covered by teflon tape to ensure efficient light collection, and optically coupled to a hybrid photo-multiplier (HPMT) model DEP PPO 475B. Signal from HPMT is processed by spectroscopy amplifier ORTEC model 672 and multichannel-buffer ORTEC 927TM. Pulse height spectrum is displayed on a PC. Several gamma ray emitting radionuclide sources were used to induce a scintillation response: ^{137}Cs (661.6 keV), ^{22}Na (511 keV, 1274 keV), ^{241}Am (59.54 keV, 13.95 keV), ^{210}Pb (46.54 keV,10.84 keV), ^{109}Cd (88.04 keV, 22.16 keV), and ^{133}Ba (81.0 keV, 160.6 keV, 276.4 keV, 302.9 keV, 356.0 keV, and 383.9 keV) (Ekström and Firestone, 2004). Only selection of ^{133}Ba lines is presented for many samples due to non-negligible interference. A 1274 keV line of ^{22}Na is not presented because of experimental setup saturation. Radioactive source was placed at a distance of several mm from the sample, depending on detection efficiency and source activity. All measurements were performed at room temperature.

For measurements of temperature dependence of light yield and decay time, a photomultiplier tube (PMT Hamamatsu R1288) and digital oscilloscope TD5032B were used. Scintillator samples were attached to the PMT R1288 which was specially designed for the well logging application by Hamamatsu. The optical grease KF-96H (Shinetsu Sillicone) was used for optical coupling and the Teflon tape was used as a reflector to collect scintillation photons. The detector was installed in the heat bath (Isuzu HPCC-48-20), the maximum temperature of which was 150 °C and the temperature was stabilized within ±0.5°C. Through the 1 cm thick heat-resistant glass, gamma-photons from radioisotopes were exciting the sample. Once γ-photon from radioisotope was detected by the sample, signals were fed into preamplifier (ORTEC 113), shaping amplifier (ORTEC 572) with typically 2 μs shaping time, and Pocket MCA (Amptek). At the same time, we measured scintillation decay profiles by an oscilloscope (Tektronix TDS5034B). From room temperature (25 °C), data were obtained with 25 °C temperature steps up to 150 °C.

III. Results

1) Crystal growth: 1-inch size Ce1%:$Gd_2Lu_1Al_2Ga_3O_{12}$, $Gd_1Lu_2Al_2Ga_3O_{12}$, $Gd_1Y_2Al_2Ga_3O_{12}$ and $Lu_2Y_1Al_2Ga_3O_{12}$ crystals with a diameter of 25 mm and length of 70-120 mm were grown. The grown crystals are shown in Fig. 1. The grown crystals are looked slightly cloudy because of the rough surface caused by gallium oxide evaporation or thermal etching. Metallic stripes on the crystal surfaces were identified as Ir deposit comes from oxidation of the crucible.

Quantitative chemical analysis of the crystals for the Ce content along the growth direction was performed by electron probe microanalysis (EPMA; JXA-8621MX, JEOL). So-called ZAF correction was used, where Z stands for atomic number, A for absorption correction factor and F for fluorescence correction factor, respectively. The Ce distributions of Ce1%:$Gd_2Lu_1Al_2Ga_3O_{12}$, $Gd_3Al_2Ga_3O_{12}$, and $Lu_2Y_1Al_2Ga_3O_{12}$ along the growth direction are shown in Fig. 2. The solidification fractions (g) of the grown crystals were 0.9, 0.55 and 0.8 for Ce1%:$Gd_2Lu_1Al_2Ga_3O_{12}$, $Gd_3Al_2Ga_3O_{12}$, and $Lu_2Y_1Al_2Ga_3O_{12}$, respectively. Here g is described as follows:

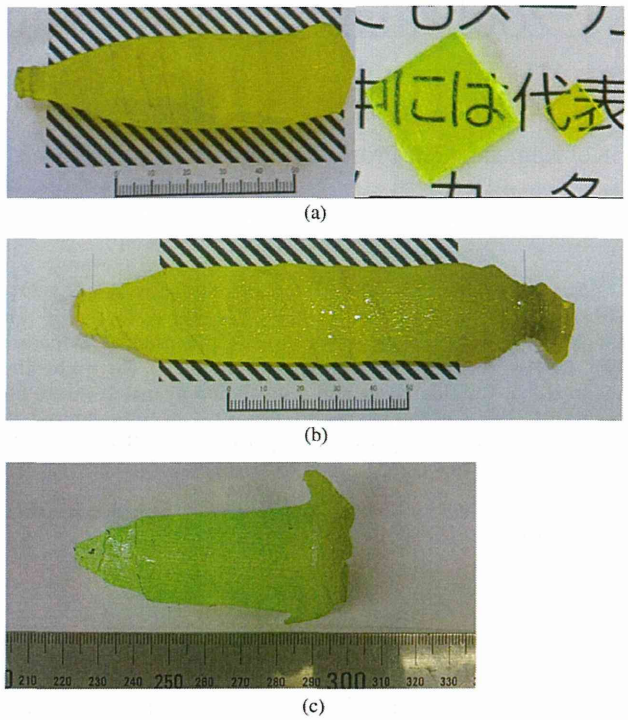

(a) (b) (c)

Fig. 1. Photographs of (a) $Gd_1Lu_2Al_2Ga_3O_{12}$ and a sample piece (b) $Gd_1Y_2Al_{1.5}Ga_{3.5}O_{12}$ and (c) $Gd_1Y_2Al_{1.5}Ga_{3.5}O_{12}$ single crystals grown by the Cz method.

$$g = (\text{mass of solidified part})/(\text{total mass of starting raw material in the crucible}).$$

Segregation coefficients of Ce were $k_{eff} = 0.46$, 0.26 and 0.10 in $Gd_3Al_2Ga_3O_{12}$, Ce1%:$Gd_2Lu_1Al_2Ga_3O_{12}$ and $Lu_2Y_1Al_2Ga_3O_{12}$, respectively. These are good agreement with that the ionic radii are Ce > Gd > Y > Lu.

2) Gamma-Ray Response: Table I shows scintillation properties of obtained samples and Ce1%:$Gd_3Al_2Ga_3O_{12}$ standard taken from 2-inch size single crystal. Smaller Gd concentration samples shows lower light yield, shorter decay time and shorter emission wavelength. Statistical occupancy in Gd site by the Lu and Y ions results in the emission band broadening. Compared to our previous report on Ce : $(Gd, Lu)_3(Al, Ga)_5O_{12}$ [1] and Ce : $(Gd, Y)_3(Al, Ga)_5O_{12}$ [2], higher light yield was obtained in the Cz grown crystals. Generally higher quality crystals can be obtained by the Cz method than that of m-PD method in the point view of lower defects such as strains and incursions, and higher homogeneity of Ce^{3+} and host composition in grown crystals [1]–[3].

An important characteristic of the Ce^{3+} luminescence center is temperature dependence of the nanosecond (prompt) decay: until the decay time value does not decrease with increasing temperature, the quantum efficiency of the center is close to one and scintillation efficiency is expected to be not decreasing as well. In Figs. 3 and 4, temperature dependences of the light output and dominant decay time were measured using the PMT

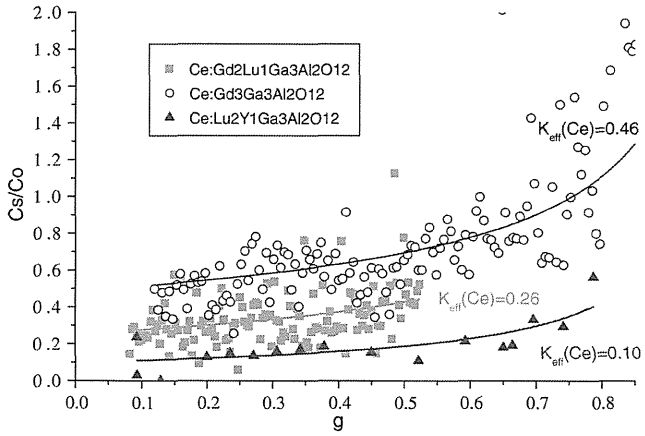

Fig. 2. Ce distributions of Ce1%:$Gd_2Lu_1Al_2Ga_3O_{12}$, $Gd_3Al_2Ga_3O_{12}$, and $Lu_2Y_1Al_2Ga_3O_{12}$ along the growth direction. Solid lines correspond to $Cs/C0 = k_{eff}(1\text{-}g)^{keff-1}$.

TABLE I
SCINTILLATION PROPERTIES OF THE SAMPLES

	Density /cm3	Emission wavelength /nm	Light yield (photon / MeV)	Decay time (ns)
Gd3Al2Ga3O12	6.65	520	46000	88ns(92%) 255ns(8%)
Lu2Gd1Ga3Al2O12	7.13	500	24000	50ns(61%) 104ns(39%)
Lu1Gd2Ga3Al2O12	6.89	510	35,000	83ns(26%) 710ns(74%)
Gd1Y2Ga3Al2O12	5.87	505	40,000	46.6ns(63%) 157ns(37%)
Lu2Y1Ga3Al2O12	6.69	490	28,000	39ns(14%) 235ns(86%)

(Hamamatsu R1288) and digital oscilloscope TD5032B excited by ^{137}Cs gamma-ray. Temperature dependence of prompt ns decay times also indicates that scintillation efficiency should not decrease until 20°C in any noticeable manner; the Gd_1Y_2 system will show the highest temperature of the onset of scintillation efficiency. These results are in good agreement with our previous report on Ce : $(Gd, Lu)_3(Al, Ga)_5O_{12}$ [1] and Ce : $(Gd, Y)_3(Al, Ga)_5O_{12}$ [2]. The Gd-rich samples have lower position of $5d_1$ level of Ce^{3+}, which secures sufficient separation of $5d_1$ level from the bottom of conduction band of the host. The onset of thermal quenching/ionization of Ce^{3+} center is certainly higher than in Gd-less samples and ensures effective scintillator functioning in room temperature applications. Increase of scintillation efficiency can be enabled also by the decrease of host band gap value, i.e., the decrease of energy for creation of one electron hole pair [14].

The dependence of relative light output on shaping time (normalized to 0.5 us value) for variously selected sample groups are shown in Fig. 5. The smallest increase of yield with shaping time is achieved for Ce : $Lu_2Gd_1Ga_3Al_2O_{12}$. It is in good agreement that Ce : $Lu_2Gd_1Ga_3Al_2O_{12}$ shows the smallest ratio of second decay component than that of others. The non-proportionality of the obtained samples is shown in Fig. 6. The

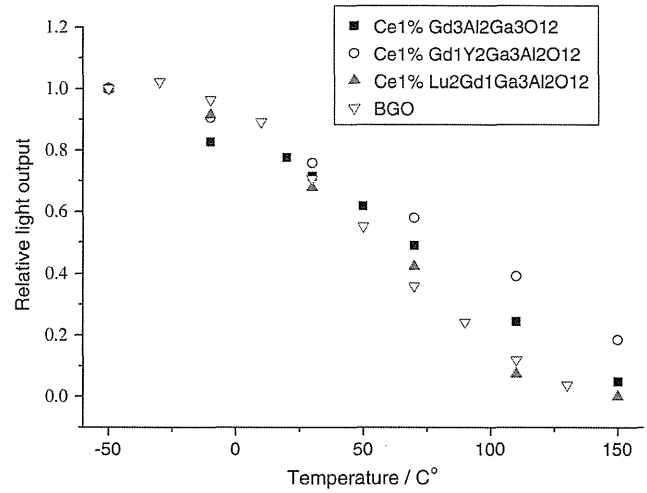

Fig. 3. Temperature dependence of relative light output measured by using the PMT excited by ^{137}Cs gamma-ray.

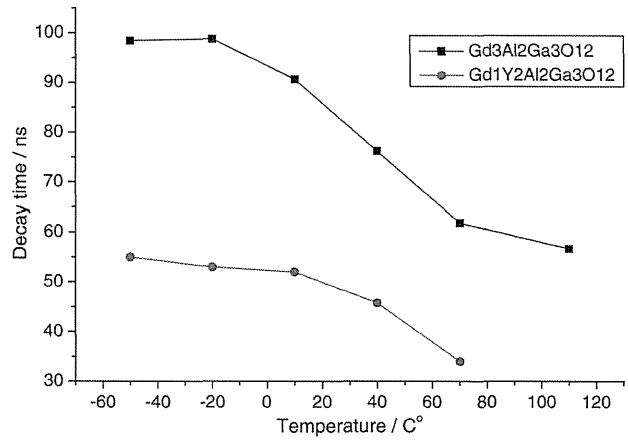

Fig. 4. Temperature dependence of decay time measured by using the PMT and digital oscilloscope excited by ^{137}Cs gamma-ray.

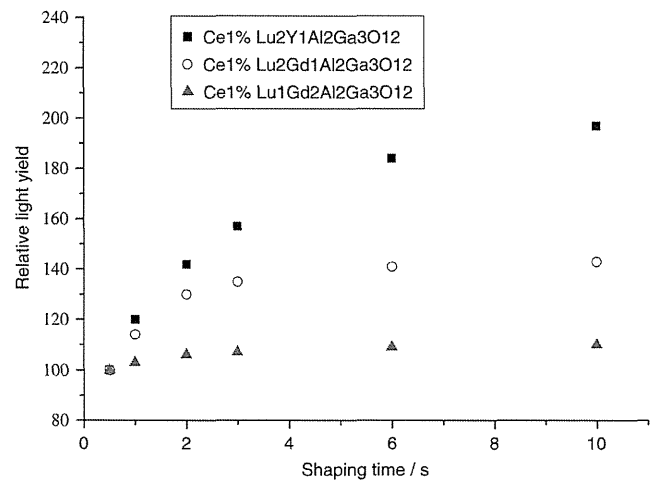

Fig. 5. Dependence of relative light out put on shaping time. Excitation by ^{137}Cs.

Ce : $Lu_2Y_1Ga_3Al_2O_{12}$ and Ce : $Lu_1Gd_2Ga_3Al_2O_{12}$ samples show better non-proportionality than that of the others.

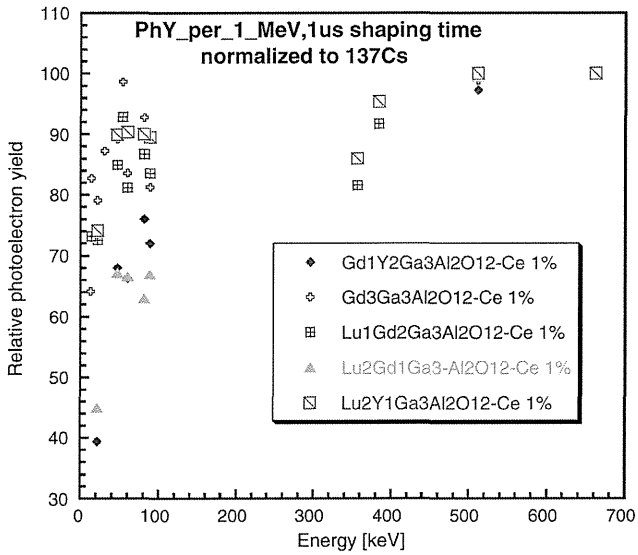

Fig. 6. Non-proportionality of the obtained samples.

IV. Conclusion

1-inch size Ce1%:$Gd_2Lu_1Al_2Ga_3O_{12}$, $Gd_1Lu_2Al_2Ga_3O_{12}$, $Gd_1Y_2Al_2Ga_3O_{12}$ and $Lu_2Y_1Al_2Ga_3O_{12}$ were grown by the Czhocralski (Cz) method. Segregation coefficients of Ce were $k_{eff} = 0.46$, 0.26 and 0.10 in Ce1%:$Gd_2Lu_1Al_2Ga_3O_{12}$, $Gd_3Al_2Ga_3O_{12}$, and $Lu_2Y_1Al_2Ga_3O_{12}$, respectively. These are in good agreement with the fact that the ionic radii are Ce > Gd > Y > Lu. Temperature dependence of light yield and scintillation decay time were investigated in the grown crystals. The Ce1%:$Gd_1Y_2Al_2Ga_3O_{12}$ shows the highest temperature stability and thermal quenching at the highest temperature among the grown crystals. The Ce1%:$Gd_1Y_2Al_2Ga_3O_{12}$ sample showed the highest light yield of around 40 000 photon/MeV. The scintillation decay time was 46.6 ns(63%) and 157 ns(37%).

Acknowledgment

The authors would like to thank the following persons for their support: Mr. Y. Nakamura in Institute of Multidisciplinary Research for Advanced Materials (IMRAM), Tohoku University and Mr. H. Uemura, Ms. K. Toguchi, Ms. M. Sasaki, and Ms. Y. Saijo in IMR.

References

[1] K. Kamada, T. Endo, K. Tsutumi, T. Yanagida, Y. Fujimoto, and A. Fukabori *et al.*, "Composition engineering in cerium-doped $(Lu, Gd)_3(Ga, Al)_5O_{12}$ single-crystal scintillators," *Cryst. Growth Design*, vol. 11, pp. 4484–4490, 2011.

[2] K. Kamada, T. Yanagida, J. Pejchal, M. Nikl, T. Endo, and K. Tsutumi *et al.*, "Scintillator-oriented combinatorial search in Ce-doped $(Y, Gd)_3(Ga, Al)_5O_{12}$ multicomponent garnet compounds," *J. Phys. D: Appl. Phys.*, vol. 44, pp. 505104–505111, 2011.

[3] K. Kamada, T. Yanagida, T. Endo, K. Tsutumi, Y. Usuki, and M. Nikl *et al.*, "2 inch diameter single crystal growth and scintillation properties of Ce : $Gd_3Al_2Ga_3O_{12}$," *J. Cryst. Growth*, vol. 352, pp. 88–90, 2012.

[4] K. Kamada, T. Yanagida, J. Pejchal, M. Nikl, T. Endo, and K. Tsutumi *et al.*, "Growth and scintillation properties of Pr doped $(Gd, Y)_3(Ga, Al)_5O_{12}$ single crystals," *IEEE Trans. Nucl. Sci.*, vol. 59, no. 5, pp. 2126–2129, 2012.

[5] K. Kamada, T. Yanagida, T. Endo, K. Tsutumi, M. Yoshino, and J. Kataoka *et al.*, "Large-size single crystal growth of Pr : $Lu_3Al_5O_{12}$ and its scintillation properties," *J. Cryst. Growth*, vol. 352, pp. 91–94, 2012.

[6] P. Prusa, K. Kamada, M. Nikl, A. Yoshikawa, and J. A. Mares, "Light yield of $(Lu, Y, Gd)_3Al_2Ga_3O_{12}$: Ce garnets," *Radiat. Meas.*, to be published.

[7] M. Nikl, A. Vedda, M. Fasoli, I. Fontana, V. V. Laguta, and E. Mihokova *et al.*, "Shallow traps and radiative recombination processes in $Lu_3Al_5O_{12}$: Ce single crystal scintillator," *Phys. Rev. B*, vol. 76, pp. 195121–195128, 2007.

[8] M. Nikl, "Energy transfer phenomena in the luminescence of wide band-gap scintillators," *Phys. Stat. Sol. (a)*, vol. 202, pp. 201–206, 2005.

[9] M. Nikl, J. Pejchal, E. Mihokova, J. A. Mares, H. Ogino, and A. Yoshikawa *et al.*, "Antisite defect-free $Lu_3(Ga_xAl_{1-x})_5O_{12}$: Pr scintillator," *Appl. Phys. Lett.*, vol. 88, pp. 141916–14198, 2006.

[10] Y. Zorenko, "Mechanism of dissipation of the excitation energy in garnet oxides doped with rare-earth ions with 4f-5d transitions," *Opt. Spectroscopy*, vol. 88, pp. 551–553, 2000.

[11] M. Fasoli, A. Vedda, M. Nikl, C. Jiang, B. P. Uberuaga, and D. A. Andersson *et al.*, "Band-gap engineering for removing shallow traps in rare-earth $Lu_3Al_5O_{12}$ garnet scintillators using Ga^{3+} doping," *Phys. Rev. B*, vol. 84, pp. 081102–081107, 2011.

[12] J. L. Wu, G. Gundiah, and A. K. Cheetham, "Structure-property correlations in Ce-doped garnet phosphors for use in solid state lighting," *Chem. Phys. Lett.*, vol. 441, pp. 250–254, 2007.

[13] N. J. Cherepy, J. D. Kuntz, Z. M. Seeley, S. E. Fisher, O. B. Drury, and B. W. Sturm *et al.*, "Transparent ceramic scintillators for gamma spectroscopy and radiography," *Proc. SPIE*, vol. 7805, pp. 780501–780505, 2010.

[14] A. Lempicki, A. Wojtowicz, and E. Berman, "Fundamental limits of scintillator performance," *Nucl. Instrum. Meth. Phys. Res. A*, vol. 333, pp. 304–311, 1993.

Fundamental study of inorganic–organic hybrid scintillator using Pr:$Lu_3Al_5O_{12}$ and plastic scintillator